View metadata, citation and similar papers at core.ac.uk
brought to you by CORE
provided by The Open Repository @Binghamton (The ORB)

Binghamton University
The Open Repository @ Binghamton (The ORB)

Physics, Applied Physics and Astronomy Faculty Scholarship

Physics, Applied Physics and Astronomy

2013

Adsorption-controlled growth of BiVO4 by molecular-beam epitaxy

S. Stoughton

M. Showak

Q. ,

P. Koirala

D. A. Hillsberry

See next page for additional authors

Follow this and additional works at: https://orb.binghamton.edu/physics_fac

Part of the Physics Commons

Recommended Citation

Stoughton, S.; Showak, M.; ,, Q.; Koirala, P.; Hillsberry, D. A.; Sallis, Shawn; Kourkoutis, L. F.; Nguyen, K.; Piper, Louis; Tenne, D. A.; Podraza, N. J.; Muller, D. A.; Adamo, C.; and Schlom, D. G., "Adsorption-controlled growth of BiVO4 by molecular-beam epitaxy" (2013). *Physics, Applied Physics and Astronomy Faculty Scholarship*. 5.
https://orb.binghamton.edu/physics_fac/5

This Article is brought to you for free and open access by the Physics, Applied Physics and Astronomy at The Open Repository @ Binghamton (The ORB). It has been accepted for inclusion in Physics, Applied Physics and Astronomy Faculty Scholarship by an authorized administrator of The Open Repository @ Binghamton (The ORB). For more information, please contact ORB@binghamton.edu.

Authors
S. Stoughton; M. Showak; Q. ,; P. Koirala; D. A. Hillsberry; Shawn Sallis; L. F. Kourkoutis; K. Nguyen; Louis Piper; D. A. Tenne; N. J. Podraza; D. A. Muller; C. Adamo; and D. G. Schlom

This article is available at The Open Repository @ Binghamton (The ORB): https://orb.binghamton.edu/physics_fac/5

Adsorption-controlled growth of BiVO4 by molecular-beam epitaxy

S. Stoughton, M. Showak, Q. Mao, P. Koirala, D. A. Hillsberry, S. Sallis, L. F. Kourkoutis, K. Nguyen, L. F. J. Piper, D. A. Tenne, N. J. Podraza, D. A. Muller, C. Adamo, and D. G. Schlom

Citation: APL Mater. **1**, 042112 (2013); doi: 10.1063/1.4824041
View online: http://dx.doi.org/10.1063/1.4824041
View Table of Contents: http://scitation.aip.org/content/aip/journal/aplmater/1/4?ver=pdfcov
Published by the AIP Publishing

Articles you may be interested in

Growth and characterization of molecular beam epitaxy-grown Bi2Te3−xSex topological insulator alloys
J. Appl. Phys. **119**, 055303 (2016); 10.1063/1.4941018

The adsorption-controlled growth of LuFe2O4 by molecular-beam epitaxy
Appl. Phys. Lett. **101**, 132907 (2012); 10.1063/1.4755765

Adsorption-controlled growth of BiMnO 3 films by molecular-beam epitaxy
Appl. Phys. Lett. **96**, 262905 (2010); 10.1063/1.3457786

Adsorption-controlled growth of EuO by molecular-beam epitaxy
Appl. Phys. Lett. **93**, 102105 (2008); 10.1063/1.2973180

Adsorption-controlled molecular-beam epitaxial growth of Bi Fe O 3
Appl. Phys. Lett. **91**, 071922 (2007); 10.1063/1.2767771

Lake Shore CRYOTRONICS
For early-stage material and device research
Explore the benefits of cryogenic device probing

Reuse of AIP Publishing content is subject to the terms at: https://publishing.aip.org/authors/rights-and-permissions. Download to IP: 128.226.37.5 On: Thu, 18 Aug 2016 18:26:46

APL MATERIALS 1, 042112 (2013)

Adsorption-controlled growth of $BiVO_4$ by molecular-beam epitaxy

S. Stoughton,[1] M. Showak,[1] Q. Mao,[2] P. Koirala,[3] D. A. Hillsberry,[4] S. Sallis,[5] L. F. Kourkoutis,[2,6] K. Nguyen,[7] L. F. J. Piper,[5,8] D. A. Tenne,[4] N. J. Podraza,[3] D. A. Muller,[2,6] C. Adamo,[1] and D. G. Schlom[1,6,a]

[1]*Department of Materials Science and Engineering, Cornell University, Ithaca, New York 14853, USA*
[2]*School of Applied and Engineering Physics, Cornell University, Ithaca, New York 14853, USA*
[3]*Department of Physics and Astronomy, University of Toledo, Toledo, Ohio 43606, USA*
[4]*Department of Physics, Boise State University, Boise, Idaho 83725, USA*
[5]*Materials Science and Engineering, Binghamton University, Binghamton, New York 13902, USA*
[6]*Kavli Institute at Cornell for Nanoscale Science, Ithaca, New York 14853, USA*
[7]*Department of Chemistry and Chemical Biology, Cornell University, Ithaca, New York, 14853, USA*
[8]*Department of Physics, Applied Physics, and Astronomy, Binghamton University, State University of New York, Binghamton, New York 13902, USA*

(Received 29 April 2013; accepted 6 September 2013; published online 11 October 2013)

Single-phase epitaxial films of the monoclinic polymorph of $BiVO_4$ were synthesized by reactive molecular-beam epitaxy under adsorption-controlled conditions. The $BiVO_4$ films were grown on (001) yttria-stabilized cubic zirconia (YSZ) substrates. Four-circle x-ray diffraction, scanning transmission electron microscopy (STEM), and Raman spectroscopy confirm the epitaxial growth of monoclinic $BiVO_4$ with an atomically abrupt interface and orientation relationship $(001)_{BiVO4} \parallel (001)_{YSZ}$ with $[100]_{BiVO4} \parallel [100]_{YSZ}$. Spectroscopic ellipsometry, STEM electron energy loss spectroscopy (STEM-EELS), and x-ray absorption spectroscopy indicate that the films have a direct band gap of 2.5 ± 0.1 eV. © *2013 Author(s). All article content, except where otherwise noted, is licensed under a Creative Commons Attribution 3.0 Unported License.* [http://dx.doi.org/10.1063/1.4824041]

Water splitting by photocatalytic materials is relevant for clean fuel generation using sunlight, i.e., artificial photosynthesis. For this application, it is critical that the band gap and band lineup are correct and also that the material does not corrode in water.[1,2] Additionally, photocatalysts that work in the visible light range are needed in order to make efficient use of solar radiation.[2,3] Recently, bismuth vanadate ($BiVO_4$) has attracted much attention as a promising photocatalyst due to its favorable band structure[4–12] and, with surface additives, reasonable stability in water.[13] $BiVO_4$ is known to exist in four different crystal structures at atmospheric pressure, though one of these (the mineral pucherite, an orthorhombic polymorph with the $CrUO_4$ structure) is only found in nature.[14] The remaining polymorphs, two with tetragonal and one with monoclinic symmetries, have all been synthesized artificially. The tetragonal polymorphs include one with the zircon structure and a band gap of ∼2.8 eV,[4,6,7] and one with the $CaWO_4$ structure and bandgap ∼2.3 eV;[6] the latter phase is the stable polymorph of $BiVO_4$ above 255°C.[14] It is the monoclinic polymorph of $BiVO_4$ with the $YNbO_4$ structure, however, that has been found to have the best photocatalytic properties in powder form, exhibiting high activity for oxygen evolution under visible light irradiation.[4,5,7,13] This monoclinic polymorph is the stable polymorph of $BiVO_4$ at room temperature and has a band gap of ∼2.4 eV.[4–12]

[a]Author to whom correspondence should be addressed. Electronic mail: schlom@cornell.edu

 ©Author(s) 2013

Reuse of AIP Publishing content is subject to the terms at: https://publishing.aip.org/authors/rights-and-permissions. Download to IP: 128.226.37.5 On: Thu, 18 Aug 2016 18:26:46

To date $BiVO_4$ has been produced in the form of powder,[4–7,10–12] polycrystalline thin films,[8,13,15–17] and single crystals.[14,18] If epitaxial thin films could be produced, $BiVO_4$ could be modified and studied in ways heretofore infeasible. For example, in epitaxial films it is possible to impose a doping profile or biaxial strain, techniques often used in the growth of epitaxial materials to manipulate the band structure. Similar strategies may make it possible to improve the photocatalytic activity of $BiVO_4$. For instance, theoretical studies have indicated that the (100) surface of monoclinic $BiVO_4$ is likely to have the greatest photocatalytic activity.[19] A prerequisite for employing the above concepts, however, is the ability to grow phase-pure epitaxial $BiVO_4$ films of good quality.

In this Letter, we report the growth of epitaxial films of the monoclinic polymorph of $BiVO_4$. These films were grown by reactive molecular-beam epitaxy (MBE) in a Veeco GEN 10 oxide MBE system under adsorption-controlled conditions in which a large excess of bismuth is supplied during growth. Within a certain temperature range, $BiVO_4$ is the only thermodynamically stable condensed phase, and excess bismuth oxide evaporates from the film surface leaving behind phase-pure $BiVO_4$. Molecular beams of bismuth and ozone, the volatile components, were supplied continuously during growth, while vanadium, the non-volatile component, was supplied in shuttered doses corresponding to individual $BiVO_4$ monolayers. This procedure is analogous to the growth conditions reported for the adsorption-controlled growth of other bismuth containing oxides by MBE including $Bi_2Sr_2CuO_6$,[20] $Bi_4Ti_3O_{12}$,[21] and $BiFeO_3$.[22]

The films were deposited onto 10×10 mm^2, (001)-oriented, single crystalline, cubic yttria-stabilized zirconia (YSZ) substrates containing 9.5 mol. % Y_2O_3. A substrate temperature of 700°C and a Bi:V flux ratio of 7.5 were used to produce the highest-quality film. Distilled ozone was supplied continuously at a background partial pressure of 1.0×10^{-6} Torr. Prior to film deposition, a quartz crystal microbalance was used to calibrate the fluxes such that the vanadium flux was 1.6×10^{13} atoms/(cm$^2 \cdot$ s) and the bismuth flux was 1.2×10^{14} atoms/(cm$^2 \cdot$ s). Although the amount of bismuth supplied was many times that required for the $BiVO_4$ structure, the excess bismuth was not incorporated into the film. As expected, for optimized growth conditions, higher Bi:V ratios were needed at higher substrate temperatures in order to compensate for the increased bismuth desorption. For the optimum film the vanadium shutter was held open for 10 s at 32 s intervals, while the bismuth and ozone were supplied continuously. These conditions correspond to an average Bi:V atomic ratio of 31.5 (Bi flux × time/V flux × time), and to a growth rate of about 2.5 Å/min. *In situ* reflection high-energy electron diffraction (RHEED) was limited to the beginning and end of growth because the 10 keV electron beam adversely affected the phase of the film.

In order to encourage epitaxial growth of monoclinic $BiVO_4$, a substrate was chosen to match both the lattice parameters and the location of ions within the structure (see the supplementary material).[23] The in-plane lattice parameters of (001) monoclinic $BiVO_4$ are $a = 5.1956$ Å and $b = 5.0935$ Å with $\gamma = 90.383°$,[18] whereas cubic YSZ with 9.5 mol. % Y_2O_3 has lattice parameter $a = 5.145$ Å.[24] This substrate provides a lattice match, $(\frac{a_{sub}-a_{film}}{a_{film}})$, of -1.0% along $[100]_{YSZ}$ and $+1.0\%$ along $[010]_{YSZ}$ to the monoclinic polymorph of $BiVO_4$ oriented $(001)[100]_{BiVO4} \parallel (001)[100]_{YSZ}$. At growth temperature, the substrate is well above the 255°C phase transition of monoclinic $BiVO_4$,[14] so if we instead consider the lattice match to the tetragonal polymorph of $BiVO_4$ with the $CaWO_4$ structure and in-plane lattice parameter at 293°C, $a = 5.147$ Å,[18] then the lattice match to YSZ at this same temperature (where YSZ has lattice parameter $a = 5.160$ Å)[25] would be $+0.3\%$. It can be seen that the lattice match of (001) $BiVO_4$ to (001) YSZ is quite good. An additional reason to anticipate epitaxial growth of $BiVO_4$ on (001) YSZ is the texture observed in polycrystalline $BiVO_4$ films grown on textured polycrystalline indium tin oxide (ITO) coated glass substrates, where local epitaxy with orientation relationship $(001)[100]_{BiVO4} \parallel (001)[100]_{ITO}$ has been inferred.[15,16] YSZ has a similar structure to ITO (isostructural if oxygen vacancy ordering is ignored) and has a superior lattice match to $BiVO_4$ than does ITO.

After growth, to assess the phase purity, epitaxy, and crystalline perfection of the $BiVO_4$ films, four-circle x-ray diffraction (XRD) was performed on a Rigaku SmartLab x-ray diffractometer using Cu-$K_{\alpha 1}$ radiation and a 220 Ge two-bounce incident-beam monochromator. In addition, cross-sectional, high-angle annular dark field (HAADF) scanning transmission electron microscopy (STEM) images were recorded on a 200kV FEI Tecnai F-20-ST equipped with a monochromator.

Reuse of AIP Publishing content is subject to the terms at: https://publishing.aip.org/authors/rights-and-permissions. Download to IP: 128.226.37.5 On: Thu, 18 Aug 2016 18:26:46

Figure 1(a) shows a $\theta-2\theta$ XRD scan of a $BiVO_4$ film grown under optimized conditions. The presence of a peak at $2\theta = 15.16^\circ$ is indicative of the presence of monoclinic $BiVO_4$ in the film as only the 002 peak of monoclinic $BiVO_4$ can occur there; the 002 peak of tetragonal $BiVO_4$ with the $CaWO_4$ structure is forbidden. The $\theta-2\theta$ XRD pattern is consistent with a single-phase monoclinic $BiVO_4$ film oriented with its (001) plane parallel to the (001) plane of the YSZ substrate. Thickness fringes around the 004 peak of monoclinic $BiVO_4$ in the $\theta-2\theta$ XRD scan give an average film thickness of 44 ± 1 nm. Additional XRD scans were performed to check for the presence of other $BiVO_4$ polymorphs; none were detected.

The crystalline perfection of the monoclinic $BiVO_4$ film was assessed by measuring the full width at half maximum (FWHM) of the rocking curve in ω and comparing it to the rocking curve of the underlying substrate. Figure 1(b) shows that the FWHM in ω of the 004 film peak is 58 arc sec (0.016°), while that of the 002 YSZ substrate peak is 40 arc sec (0.011°).

To check for epitaxy and establish the epitaxial orientation relationship, a ø-scan of the {301} family of planes of monoclinic $BiVO_4$ was made (Fig. 1(c)). This family of planes was chosen because the peaks are intense and unambiguous. In other words, the 301-type peaks are sufficiently far from other film and substrate peaks in χ or 2θ to avoid overlap. The ø-scan indicates that the $BiVO_4$ film is epitaxial with orientation relationship $(001)_{BiVO4} \parallel (001)_{YSZ}$ with $[100]_{BiVO4} \parallel [100]_{YSZ}$. If the monoclinic $BiVO_4$ were an untwinned single crystal, only two 301-type peaks would be observed in the ø-scan. The fact that instead four peaks appear in the scan implies that the sample contains 90° in-plane rotational twinning, which is expected considering the 4-fold symmetry of the (001) YSZ substrate.

The epitaxial orientation relationship and the film thickness were corroborated by HAADF STEM imaging. In addition, STEM elucidated the film microstructure. The HAADF STEM images in Fig. 2 reveal the film/substrate interface to be abrupt and the film to be free of amorphous content, which if present would not give rise to additional peaks in XRD and thus could not be ruled out by XRD alone. The film is not continuous, but rather composed of 200−500 nm wide islands (Fig. 2(d)), with island thicknesses in the range of 40−56 nm. This is consistent with the thickness fringes in the 2θ XRD scan. The fractional coverage of film on the substrate is $70 \pm 5\%$ (see the supplementary material).[23] The projection of the atom positions observed by STEM (Fig. 2(b)) also corresponds well with the crystallographic model of the targeted epitaxial alignment between (001) $BiVO_4$ and (001) YSZ (see the supplementary material).[23]

Raman spectroscopy of the film confirms the monoclinic polymorph. Raman spectra were measured in backscattering geometry normal to the film surface using a Jobin Yvon T64000 triple spectrometer equipped with a liquid nitrogen cooled multichannel charge coupled device detector. The 441.6 nm (2.81 eV) line of a He-Cd laser was used for excitation since the energy is close to the band gap of $BiVO_4$ and therefore produces a strong signal. Spectra were recorded at both room temperature and at 10 K using a variable temperature closed cycle helium cryostat. As shown in Fig. 3, the most intense peak, observed at 820 cm^{-1} and 811 cm^{-1} at 10 K and 300 K, respectively, corresponds to the symmetric V–O stretching mode (A_g symmetry, stronger in parallel polarization configuration), while the peaks at 331 cm^{-1} and 366 cm^{-1} are attributed to the symmetric bending modes of the VO_4 units. Prior studies have shown that the position of these two peaks can be used to distinguish among the various polymorphs of $BiVO_4$, and the measured peak positions in our film correspond well to expected results for the monoclinic polymorph.[26] The peak at 218 cm^{-1} can be attributed to one of the external lattice modes of $BiVO_4$.[27] The strongest peak of the YSZ substrate appears near 615 cm^{-1}, which is consistent with the literature.[28] Although the peaks in the lower frequency range (below 450 cm^{-1}) are weaker and may overlap with some YSZ features, there is no doubt that the 218 cm^{-1}, 331 cm^{-1}, and 366 cm^{-1} peaks originate from the $BiVO_4$ film. These $BiVO_4$ peaks (like the strongest peak at 820 cm^{-1}) are enhanced when the excitation laser energy is close to the resonance near the bandgap of $BiVO_4$, while the YSZ substrate features do not show such enhancement.

The band gap, optical properties, and bonding characteristics of the epitaxial monoclinic $BiVO_4$ film were studied using spectroscopic ellipsometry, STEM electron energy loss spectroscopy (STEM-EELS),[36] and x-ray emission and absorption spectroscopy (XES/XAS). The XES/XAS were in agreement with earlier studies of pellets,[10] and the XAS and STEM-EELS confirmed a

Reuse of AIP Publishing content is subject to the terms at: https://publishing.aip.org/authors/rights-and-permissions. Download to IP: 128.226.37.5 On: Thu, 18 Aug 2016 18:26:46

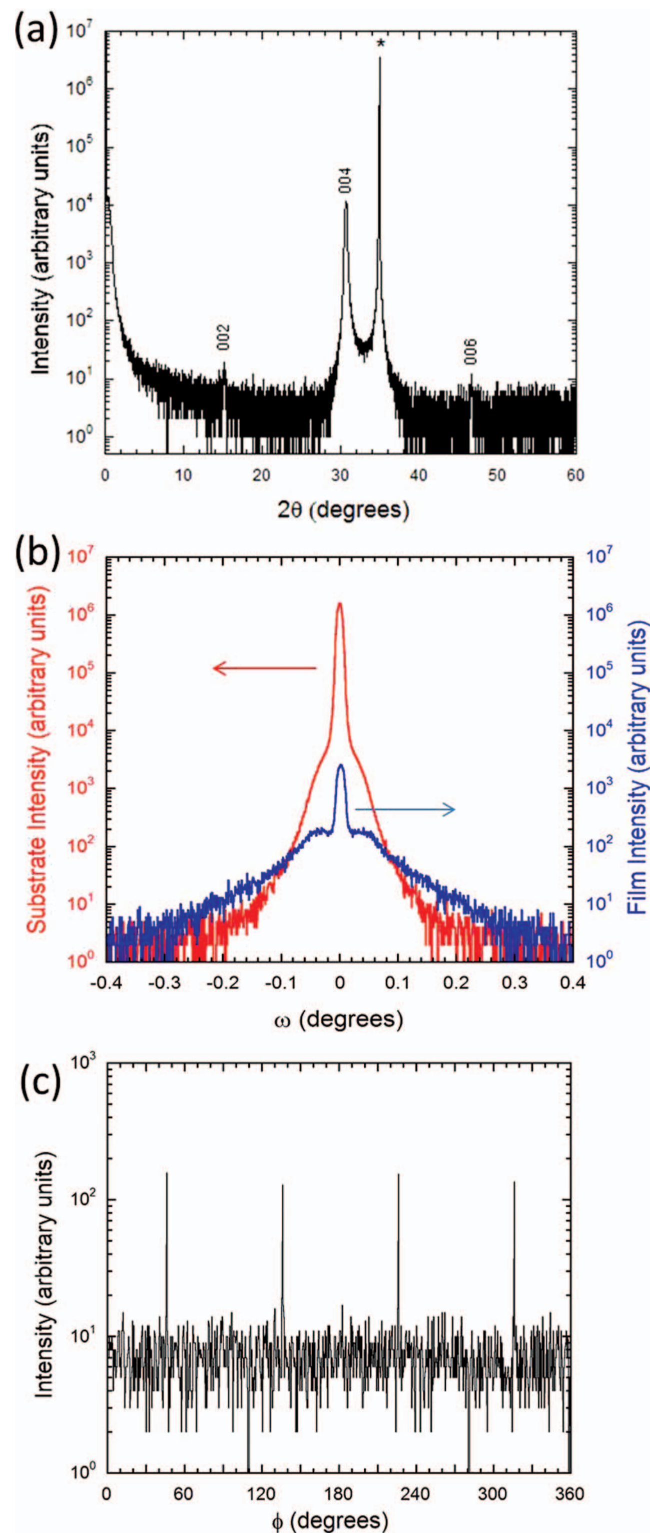

FIG. 1. (a) $\theta-2\theta$ x-ray diffraction scan of $BiVO_4$ grown on a (001) YSZ substrate. The peak labeled with * in (a) corresponds to the 002 YSZ substrate peak. (b) Rocking curve (ω scan) of the 004 $BiVO_4$ film peak overlaid on the 002 YSZ substrate peak. The FWHM of the $BiVO_4$ peak is 0.016° and that of the substrate is 0.011°. (c) ø-scan of the 301 $BiVO_4$ reflection at $2\theta = 54.36°$ and $\chi = 8.42°$. $\chi = 90°$ is defined as perpendicular to the plane of the substrate. $ø = 0°$ is aligned to be parallel to the 202 in-plane direction of YSZ. These scans show that the film is the monoclinic polymorph of $BiVO_4$ and is epitaxially oriented to the YSZ substrate with 90° in-plane twinning.

Reuse of AIP Publishing content is subject to the terms at: https://publishing.aip.org/authors/rights-and-permissions. Download to IP: 128.226.37.5 On: Thu, 18 Aug 2016 18:26:46

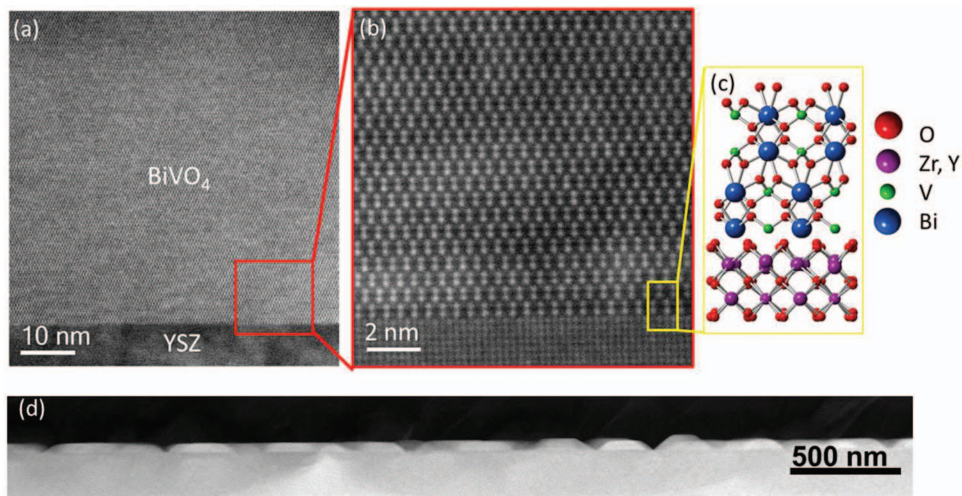

FIG. 2. Cross-sectional HAADF-STEM images of the same monoclinic $BiVO_4$ film analyzed in Fig. 1. The bright positions in the $BiVO_4$ layer correspond to the projected positions of the Bi ions, and the bright positions in the YSZ layer are the Y/Zr ions. The model of the expected epitaxial alignment between (001) $BiVO_4$ and (001) YSZ is shown in (c), which corresponds to the region enclosed within the yellow-rectangle in (b). (d) Low magnification image showing the islanded film.

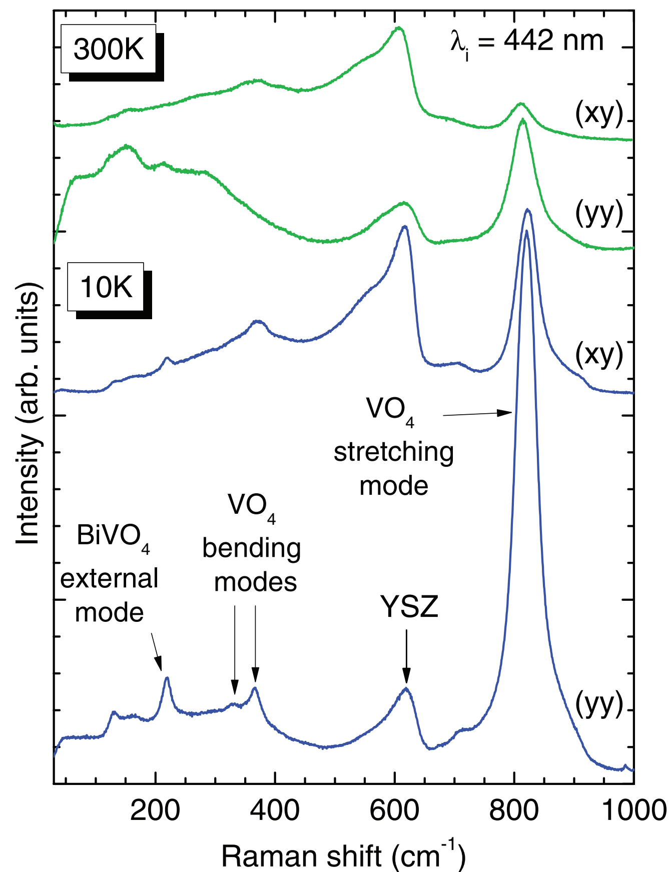

FIG. 3. Raman spectra of the same $BiVO_4$ film analyzed in Fig. 1 at 10 K and 300 K. Notations (*yy*) and (*xy*) indicate parallel and perpendicular polarizations of incident and scattered light, respectively. The peak labeled YSZ can be attributed to Raman scattering from the YSZ substrate.

Reuse of AIP Publishing content is subject to the terms at: https://publishing.aip.org/authors/rights-and-permissions. Download to IP: 128.226.37.5 On: Thu, 18 Aug 2016 18:26:46

V5+ charge state throughout the film (see the supplementary material).[23] Room temperature ellipsometric spectra (in Δ, ψ) were collected after growth using a variable-angle rotating-compensator multichannel spectroscopic ellipsometer.[29,30] Multiple sample orientations were studied at angles of incidence of $\psi = 60^\circ$ and 70° over a spectral range from 0.75 to 6.0 eV. The complex dielectric function spectra ($\varepsilon = \varepsilon_1 + i\varepsilon_2$) and microstructural parameters (film thickness, d_b, and surface roughness thickness, d_s) were extracted using a least squares regression analysis and an unweighted error function,[31] σ, to fit the experimental ellipsometric spectra to an optical model. The system was modeled as semi-infinite YSZ substrate / $BiVO_4$ film/surface roughness/air ambient, where free parameters correspond to the $BiVO_4$ film and surface roughness and a parameterization of ε for $BiVO_4$. The optical properties of the $BiVO_4$ film and surface roughness layers are represented using the Bruggeman effective medium approximation[32] with fixed fractions of "dense" $BiVO_4$ material (f_{BiVO4}) and void in order to account for fractional coverage. f_{BiVO4} was fixed at 0.65, 0.70, and 0.75 to evaluate the impact of the ±5% uncertainty in the 70% surface coverage. The void fraction in the surface roughness was fixed at 0.675, 0.65, and 0.625, respectively, so that the properties of this layer represented equal contributions from void and the film (itself containing some fraction of voids).

The low (0.75 to 1.3 eV) and high (2.6 to 6.0 eV) photon energy ranges of the ellipsometric spectra were fit using the same structural model and common thickness parameters (d_b, d_s), but using different parameterizations of ε. For the low energy range, parameterization of ε consisted of a Sellmeier[33] oscillator, as there are no strong absorption features present. In the high-energy range, the parameterization consisted of four oscillators based on critical point parabolic band (CPPB) approximations[34] as critical point features are present above the band gap. A constant additive term to ε_1 was also included for each. The region from 1.3 to 2.6 eV is in the vicinity of the band gap where the choice of parameterization of ε depends on how $\varepsilon_2 \rightarrow 0$ (indirect or direct band gap behavior) and on the Urbach tail absorption for crystalline materials. Since these choices impose constraints that can cause inaccurate bias towards a particular line shape in extracted parameters, this region was excluded and physically realistic models were adopted for the higher and lower energy regions.

First, the film thickness (47.6 ± 0.3 nm) and surface layer thickness (0.3 ± 0.1 nm) for each fixed f_{BiVO4} in the film layer were obtained using this approach; the results were found to correlate well with XRD and STEM observations. Then, the thicknesses were fixed and ε was extracted by numerical inversion over the full spectral range. The results for $f_{BiVO4} = 0.70$ are shown in Fig. 4(a). ε obtained assuming $f_{BiVO4} = 0.65$ and 0.75 yielded similar line shapes, but approximately 10% higher or lower amplitudes, respectively. It should be noted that although $BiVO_4$ is anisotropic, an isotropic approximation for ε was used to maintain the highest signal-to-noise ratio in the extracted values. Parameterization of ε_2 shows the lowest energy critical point at 2.74 ± 0.01 eV with an additional point slightly higher at 2.93 ± 0.02 eV. Theoretical calculations suggest that these features may be attributed to transitions between the V 3*d* and O 2*p* electrons.[9]

After ε was obtained, the absorption coefficient, α, was determined for each assumed f_{BiVO4} with results for $f_{BiVO4} = 0.70$ shown in Fig. 4(b). $\alpha^{1/2}$ and α^2 were plotted as functions of photon energy and extrapolated using a linear relationship to $\alpha^{1/2}$ $[\alpha^2] = 0$ in order to identify the indirect (direct) band gap.[35] The direct gap is determined from a single slope of $\alpha^2 = 0$, as shown in the inset of Fig. 4(b). Linearity in the spectral region near $\alpha \sim 10^4{-}10^5$ cm^{-1} yields direct band gap values of 2.52 ± 0.05 eV ($f_{BiVO4} = 0.65$), 2.54 ± 0.05 eV ($f_{BiVO4} = 0.70$), and 2.56 ± 0.05 eV ($f_{BiVO4} = 0.75$). The lowest energy critical point at 2.74 eV may be considered the upper limit for band gap extrapolation.

The significant absorption observed below the band gap obtained from spectroscopic ellipsometry measurements may be attributed to the fractional film coverage observed with STEM. The optical model assumed average fractional coverage, which is valid when the spacing between $BiVO_4$ regions is small compared to the wavelength of the probing light. Larger features can result in scattering, which may lead to the artificially high values of absorption below the band gap that were observed. To determine the band gap independently of the morphology, an electron energy loss spectrum (EELS) of the same $BiVO_4$ film was recorded from a spot with ~4 nm diameter in the interior of the monoclinic $BiVO_4$ layer, as indicated in the cross-sectional STEM image (inset of Fig. 4(c)). EELS measures $Im(-1/\varepsilon) = \varepsilon_2 / \left(\varepsilon_1^2 + \varepsilon_2^2\right)$, and the resulting spectrum is shown in

Reuse of AIP Publishing content is subject to the terms at: https://publishing.aip.org/authors/rights-and-permissions. Download to IP: 128.226.37.5 On: Thu, 18 Aug 2016 18:26:46

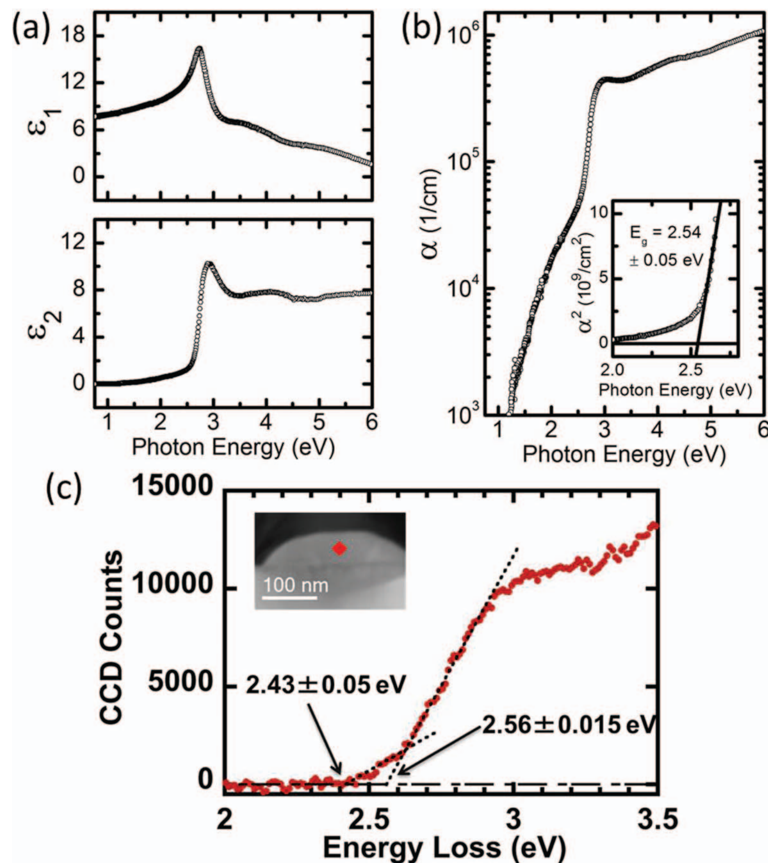

FIG. 4. (a) Complex dielectric function spectra ($\varepsilon = \varepsilon_1 + \varepsilon_2$) and (b) absorption coefficient of the same monoclinic $BiVO_4$ film studied in Fig. 1 extracted assuming a film coverage of 70% (i.e., 70% $BiVO_4$, 30% void). The inset to (b) shows the direct band gap, E_g, obtained by linearizing $\alpha^2 = 0$ eV. (c) Spatially resolved monochromated EELS from the interior of the same $BiVO_4$ film, viewed in cross-section (inset). The background was corrected with a power-law fit from 1.5 to 2 eV, with the flat region in the band gap from 2 to 2.4 eV showing the precision of the fit. The energy resolution, as determined from the FWHM of the zero loss peak, was 0.14 eV.

Fig. 4(c). After fitting a power law background to the tails of the unscattered beam, the band gap could be resolved and estimated using linear extrapolation. Depending on the extrapolation, the gap would be 2.43 ± 0.05 eV for the small knee or 2.56 ± 0.015 eV for the main peak. The absorption giving rise to the lower band gap (2.43 eV) could arise from a small concentration of point defects such as oxygen vacancies in the $BiVO_4$ film or it could be due to surface damage that occurs during STEM sample preparation.

In summary, epitaxial thin films of monoclinic $BiVO_4$ have been grown on cubic (001) YSZ substrates using adsorption-controlled MBE. XRD, STEM, and Raman spectroscopy confirm that the sample is epitaxial, phase-pure monoclinic $BiVO_4$. Global and localized spectroscopic probes indicate that the epitaxial monoclinic $BiVO_4$ film has a direct band gap of 2.5 ± 0.1 eV.

This work was supported as part of the Energy Materials Center at Cornell (EMC^2), an Energy Frontier Research Center funded by the U.S. Department of Energy, Office of Science, Office of Basic Energy Sciences under Grant No. DE-SC0001086. This work also made use of the electron microscopy facility of the Cornell Center for Materials Research (CCMR) supported by the National Science Foundation under Award No. DMR-1120296. This work was performed in part at the Cornell NanoScale Facility, a member of the National Nanotechnology Infrastructure Network, which is supported by the National Science Foundation (Grant ECCS-0335765). Raman studies at Boise State University have been supported by NSF under Grant No. DMR-1006136. The National

Reuse of AIP Publishing content is subject to the terms at: https://publishing.aip.org/authors/rights-and-permissions. Download to IP: 128.226.37.5 On: Thu, 18 Aug 2016 18:26:46

Synchrotron Light Source is supported by the U.S. Department of Energy, Contract No. DE-AC02-98CH10886. L.F.J.P. and S.S. acknowledge support from the Faculty/Student Research Support Program at the NSLS. We thank Professor Kevin Smith for use of his end-station at the NSLS.

[1] O. Khaselev and J. Turner, Science **280**, 425 (1998).
[2] T. Bak, J. Nowotny, M. Rekas, and C. C. Sorrell, Int. J. Hydrogen Energy **27**, 991 (2002).
[3] K. Sayama, A. Nomura, T. Arai, T. Sugita, R. Abe, M. Yanagida, T. Oi, Y. Iwasaki, Y. Abe, and H. Sugihara, J. Phys. Chem. B **110**, 11352 (2006).
[4] A. Kudo, K. Omori, and H. Kato, J. Am. Chem. Soc. **121**, 11459 (1999).
[5] S. Tokunaga, H. Kato, and A. Kudo, Chem. Mater. **13**, 4624 (2001).
[6] M. W. Stoltzfus, P. M. Woodward, R. Seshadri, J.-H. Klepeis, and B. Bursten, Inorg. Chem. **46**, 3839 (2007).
[7] H. M. Zhang, J. B. Liu, H. Wang, W. X. Zhang, and H. Yan, J. Nanopart. Res. **10**, 767 (2008).
[8] H. Luo, A. Mueller, T. McCleskey, A. Burrell, E. Bauer, and Q. Jia, J. Phys. Chem. C **112**, 6099 (2008).
[9] A. Walsh, Y. Yan, M. N. Huda, M. M. Al-Jassim, and S.-H. Wei, Chem. Mater. **21**, 547 (2009).
[10] D. J. Payne, M. D. M. Robinson, R. G. Egdell, A. Walsh, J. McNulty, K. E. Smith, and L. F. J. Piper, Appl. Phys. Lett. **98**, 212110 (2011).
[11] Y. Hu, D. Li, Y. Zheng, W. Chen, Y. He, Y. Shao, X. Fu, and G. Xiao, Appl. Catal., B **104**, 30 (2011).
[12] W. J. Jo, J.-W. Jang, K.-J. Kong, H. J. Kang, J. Y. Kim, H. Jun, K. P. S. Parmar, and J. S. Lee, Angew. Chem., Int. Ed. **51**, 3147 (2012).
[13] J. A. Seabold and K.-S. Choi, J. Am. Chem. Soc. **134**, 2186 (2012).
[14] J. D. Bierlein and A. W. Sleight, Solid State Commun. **16**, 69 (1975).
[15] M. Zhou, S. Zhang, Y. Sun, C. Wu, M. Wang, and Y. Xie, Chem. Asian J. **5**, 2515 (2010).
[16] M. Zhou, J. Bao, W. Bi, Y. Zeng, R. Zhu, M. Tao, and Y. Xie, ChemSusChem **5**, 1420 (2012).
[17] Q. Jia, K. Iwashina, and A. Kudo, Proc. Natl. Acad. Sci. U.S.A. **109**, 11564 (2012).
[18] A. W. Sleight, H. Y. Chen, A. Ferretti, and D. E. Cox, Mater. Res. Bull. **14**, 1571 (1979).
[19] Z. Zhao, Z. Li, and Z. Zou, Phys. Chem. Chem. Phys. **13**, 4746 (2011).
[20] S. Migita, Y. Kasai, H. Ota, and S. Sakai, Appl. Phys. Lett. **71**, 3712 (1997).
[21] C. D. Theis, J. Yeh, D. G. Schlom, M. E. Hawley, G. W. Brown, J. C. Jiang, and X. Q. Pan, Appl. Phys. Lett. **72**, 2817 (1998).
[22] J. F. Ihlefeld, A. Kumar, V. Gopalan, D. G. Schlom, Y. B. Chen, X. Q. Pan, T. Heeg, J. Schubert, X. Ke, P. Schiffer, J. Orenstein, L. W. Martin, Y. H. Chu, and R. Ramesh, Appl. Phys. Lett. **91**, 071922 (2007).
[23] See supplementary material at http://dx.doi.org/10.1063/1.4824041 for depictions of the crystal structure of the film and substrate, air SEM analysis from which fractional coverage was estimated, and x-ray spectroscopy results confirming bonding states of film atoms.
[24] Calculated by interpolation (assuming Vegard's law) from the cubic lattice constants of YSZ with 9 and 10 mol% Y_2O_3 reported by M. Yashima, S. Sasaki, M. Kakihana, Y. Yamaguchi, H. Arashi, and M. Yoshimura, Acta Crystallogr., Sect. B **50**, 663 (1994).
[25] Calculated by interpolating the thermal expansion data for YSZ reported by J. W. Adams, H. H. Nakamura, R. P. Ingel, and R. W. Rice, J. Am. Ceram. Soc. **68**, C-228 (1985).
[26] R. L. Frost, D. A. Henry, M. L. Weier, and W. Martens, J. Raman Spectrosc. **37**, 722–732 (2006).
[27] M. Gotic, S. Music, M. Ivanda, M. Soufek, and S. Popovic, J. Mol. Struct. **744–747**, 535 (2005).
[28] J. Cai, C. Raptis, Y. S. Raptis, and E. Anastassakis, Phys. Rev. B **51**, 201 (1995).
[29] J. Lee, P. I. Rovira, I. An, and R. W. Collins, Rev. Sci. Instrum. **69**, 1800 (1998).
[30] B. Johs, J. A. Woollam, C. M. Herzinger, J. Hilfiker, R. Synowicki, and C. L. Bungay, in *Critical Reviews of Optical Science and Technology, Optical Metrology*, edited by G. A. Al-Jumaily (SPIE Publishing, Bellingham, WA, 1999), Vol. CR72, pp. 29–58.
[31] Y. Cong, I. An, K. Vedam, and R. W. Collins, Appl. Opt. **30**, 2692 (1991).
[32] H. Fujiwara, J. Koh, P. I. Rovira, and R. W. Collins, Phys. Rev. B **61**, 10832 (2000).
[33] R. W. Collins and A. S. Ferlauto, in *Handbook of Ellipsometry*, edited by H. G. Tompkins and E. A. Irene (William Andrew, Norwich, NY, 2005), pp. 125–129.
[34] D. E. Aspnes, in *Handbook on Semiconductors*, edited by M. Balkanski (North Holland, Amsterdam NL, 1980), Vol. 2, pp. 125–127.
[35] J. I. Pankov, *Optical Processes in Semiconductors* (Dover, New York, 1975), p. 37.
[36] L. F. Kourkoutis, Y. Hotta, T. Susaki, H. Y. Hwang, and D. A. Muller, Phys. Rev. Lett. **97**, 256803 (2006).

Reuse of AIP Publishing content is subject to the terms at: https://publishing.aip.org/authors/rights-and-permissions. Download to IP: 128.226.37.5 On: Thu, 18 Aug 2016 18:26:46